Title

Ceramide synthase TLCD3B is a novel gene associated with human recessive retinal dystrophy.

Journal

Genetics in Medicine, 23(3)

Authors

Bertrand, Renae
Wang, Jun
Xiong, Kaitlyn
et al.

Publication Date

2021-03-01

DOI

10.1038/s41436-020-01003-x

Peer reviewed

HHS Public Access

Author manuscript

Genet Med. Author manuscript; available in PMC 2021 April 20.

Published in final edited form as:

Genet Med. 2021 March ; 23(3): 488–497. doi:10.1038/s41436-020-01003-x.

Ceramide synthase *TLCD3B* is a novel gene associated with human recessive retinal dystrophy

Renae Elaine Bertrand, B.S.[1,2], **Jun Wang, Ph.D.**[2,3], **Kaitlyn H. Xiong, B.S.**[2,4], **Chinthana Thangavel**[2,4], **Xinye Qian, B.A.**[1,2], **Rola Ba-Abbad, FRCS, Ph.D.**[5], **Qingnan Liang, M.S.**[1,2], **Renata T. Simões**[6], **Shirley A. M. Sampaio**[7], **Keren J. Carss, Ph.D.**[8,9], **F. Lucy Raymond, M.D. Ph.D.**[8,10], **Anthony G. Robson, M.Sc. Ph.D.**[11], **Andrew R. Webster, FRCOphth**[5,11], **Gavin Arno, Ph.D.**[5,11,12], **Fernanda Belga Ottoni Porto, M.D. Ph.D.**[7], **Rui Chen, Ph.D.**[2,3,*]

[1]Verna and Marrs McLean Department of Biochemistry and Molecular Biology, Baylor College of Medicine, Houston, TX 77030, USA

[2]Human Genome Sequencing Center, Baylor College of Medicine, Houston, TX 77030, USA

[3]Department of Molecular and Human Genetics, Baylor College of Medicine, Houston, TX 77030, USA

[4]Department of BioSciences, Rice University, Houston, TX 77005, USA

[5]Moorfields Eye Hospital, London, EC1V 2PD, UK

[6]Instituto de Ensino e Pesquisa da Santa Casa de Belo Horizonte (IEP/SCBH), Minas Gerais, Brazil

[7]INRET Clínica e Centro de Pesquisa, Belo Horizonte, Minas Gerais, Brazil

[8]Department of Haematology, University of Cambridge, Cambridge, UK

[9]NIHR BioResource-Rare Diseases, Cambridge University Hospitals, Cambridge Biomedical Campus, Cambridge, UK

[10]Department of Medical Genetics, Cambridge Institute for Medical Research, University of Cambridge, Cambridge, UK

[11]UCL Institute of Ophthalmology, London, EC1V 9EL, UK

[12]Great Ormond Street Hospital for Children, London, UK

Abstract

Purpose—Previous studies suggest that ceramide is a proapoptotic lipid as high levels of ceramides can lead to apoptosis of neuronal cells, including photoreceptors. However, no pathogenic variant in ceramide synthases has been identified in human patients and knockout of various ceramide synthases in mice has not led to photoreceptor degeneration.

*Rui Chen, 713-798-5194, ruichen@bcm.edu.

CONFLICT OF INTEREST STATEMENT

All authors state that they have no conflicts of interest to disclose.

Methods—Exome sequencing was used to identify candidate disease genes in patients with vision loss as confirmed by standard evaluation methods, including electroretinography (ERG) and optical coherence tomography. The vision loss phenotype in mice was evaluated by ERG and histological analyses.

Results—Here we have identified four patients with cone-rod dystrophy or maculopathy from three families carrying pathogenic variants in *TLCD3B*. Consistent with the phenotype observed in patients, the *Tlcd3b*$^{KO/KO}$ mice exhibited a significant reduction of the cone photoreceptor light responses, thinning of the outer nuclear layer, and loss of cone photoreceptors across the retina.

Conclusion—Our results provide the first link between loss-of-function variants in a ceramide synthase gene and human retinal dystrophy. Establishment of the *Tlcd3b* knockout murine model, the first *in vivo* photoreceptor cell degeneration model due to loss of a ceramide synthase, will provide a unique opportunity in probing the role of ceramide in survival and function of photoreceptor cells.

Keywords

Retinal degeneration; ceramide synthase; cone-rod degeneration; novel disease gene; TLCD3B

INTRODUCTION

Inherited retinal dystrophies (IRDs) are a diverse set of disorders whose primary site of pathology is often, but not exclusively, the rod and/or cone photoreceptors. Causative genes vary in their involvement of each disorder; at least 250 genes have been identified to underlie retinal dystrophy (https://sph.uth.edu/retnet). The advances in next-generation sequencing and its applications for molecular diagnostics for individuals with IRDs have increased the diagnostic yield up to 70%[1]. Identifying the molecular diagnosis in these cases assists in clinical management of patients, and future inclusion in therapeutic trials. Clinical investigation involving detailed imaging and electrophysiology in humans, in concert with in-depth phenotyping of relevant animal models can provide insights into the basic pathophysiology.

There is clinical heterogeneity within and overlap between different IRDs. Cone-rod dystrophy (CRD) and maculopathy are two broad diagnoses that encompass varying phenotypes and it is possible for a patient's diagnosis to change as the disease progresses. CRD and maculopathy are IRDs characterized by a shared clinical presentation of reduced central vision and significant peripheral cone dysfunction more than rod system dysfunction evident on electroretinography (ERG), indicating significant cone photoreceptor involvement in the pathology[23]. It has been reported that homeostasis of ceramide plays an important role in retinal neuron survival. Ceramides are a class of sphingolipids that are abundant in cell membranes and serve as important second messengers. Ceramide is generated through four pathways, *de novo* synthesis, the salvage pathway, the sphingomyelinase pathway, and the exogenous ceramide-recycling pathway, where ceramide synthases participate in all but the sphingomyelinase pathway[45]. In mammals, six ceramide synthases (CERS), CERS1–6, each regulate the formation of a specific set of ceramides, which mediate distinct functions[5]. There is redundancy in the ceramides synthesized by each

synthase, but no ceramide synthase can completely compensate for another[6–10]. Ceramides have been shown to mediate many cell-stress responses, including apoptosis[511–13]. Interestingly, both high and low levels of ceramides have been linked to apoptosis. Long-chain ceramides are known to be pro-apoptotic in many contexts, including the retina and brain[11–15]. A reduction in ceramide levels has been previously linked to neurodegeneration, specifically of Purkinje cells in the cerebellum of *CerS1* deficient mice[10]. So far, pathogenic variants in ceramide synthases have been associated with diseases, such as epilepsy[61617], but not with retinal degeneration in patients, and previous ceramide synthase knockout mouse models have not shown retinal degeneration phenotypes[18]. Previous studies have identified *Ceramide Kinase Like* (*CERKL*) to be a retinal degeneration gene[19], but it has been established that CERKL does not participate in sphingolipid metabolism[2021]. In addition to the canonical ceramide synthases, it has been reported that the protein encoded by the TRAM/LAG1/CLN8 Domain 3B (*TLCD3B,* formally known as *FAM57B*) gene also has ceramide synthase activity. An *in vitro* study showed that *TLCD3B* can function as a novel ceramide synthase and is responsible for synthesis of C16-, C18-, and C20-ceramides[22]. The *in vivo* function of *TLCD3B* has not yet been confirmed and its connection with the central nervous system has not yet been investigated.

While it has been established that maintenance of ceramide levels is important for retinal cell survival, the roles of ceramides and ceramide synthases are not well studied in the retina. In this study, we have identified pathogenic variants in *TLCD3B* in four patients from three unrelated families diagnosed with CRD or maculopathy. Consistent with the patient phenotype, disruption of *Tlcd3b* in mice leads to cone photoreceptor degeneration. Our results provide the first direct link between defects in a ceramide synthase and human retinal degeneration.

MATERIALS AND METHODS

Ethics Statement

Informed consent was acquired from all of the Brazilian patients and participating family members who chose to participate. All of the procedures were approved by appropriate institutional review boards and ethics committees (Santa Casa de Belo Horizonte Research Ethics Committee CAAE: 11168613.0.0000.5138), and adhered to the tenets of the declaration of Helsinki. For Patient C.IV.3 (GC18125), all diagnostic procedures were approved by the UK Research Ethics Committee, granted by the Cambridge South REC, informed consent was obtained from all patients or guardians, and procedures adhered to the tenets of the declaration of Helsinki. All animal procedures and experiments conformed to the IACUC-approved protocol.

Bioinformatics Analysis

Patients A.II.1, A.II.2 and B.II.1 were subjected to exome sequencing. After exome sequencing, BWA v.0.7.12[23] was used to map the reads to the human genome assembly hg19. The retinal disease-causing variants were identified as previously described[24]. Details of the analysis are available in the supplemental methods.

Patient C.IV.3 was subjected to genome sequencing, which was carried out as part of the NIHR BioResoirce – Rare Disease study as previously descibed[25]. Rare variant interrogation was performed using a curated virtual gene panel of known retinal dystrophy genes to exclude a known cause of disease. Following this, rare, biallelic loss of function variants in genes not harbouring homozygous null alleles in the ExAC dataset were interrogated[25]. Variant filtering and prioritization were performed as previously described[25].

Clinical Evaluation

All Brazilian patients and family members have been examined by the same care provider (author FBOP), including best-corrected visual acuity (BCVA), slit-lamp biomicroscopy, dilated-pupil fundus examination, cycloplegic refraction, optical coherence tomography (OCT) (Cirrus HD-OCT, Carl Zeiss Meditec, Germany), fundus imaging, fundus autofluorescence (FAF) imaging (Topcon retinal camera TRC-NW8, Topcon Co., Japan), and full-field ERG (ffERG) (UTAS Sunburst, LKC Tecknologies, USA).

Patient C.IV.3 (GC18125) underwent examinations at the inherited Eye Disease clinics at Moorfields Eye Hospital, London, UK, which included BCVA, dilated fundus examination, OCT (Spectralis HRA +OCT, Heidelberg Engineering, Germany), FAF imaging (Spectralis HRA +OCT, Heidelberg Engineering, Germany), and wide-field fundus imaging (Optos plc, United Kingdom). Detailed clinical evaluation information is available in the supplementary materials and methods.

Animals

All animal phenotyping materials and methods are standard procedure and can be found in the supplementary materials and methods. Fam57b$^{em1(IMPC)Bay}$/Mmnc mice in the C57BL/6NJ background were obtained from the Knockout Mouse Project (KOMP) at Baylor College of Medicine. All mice were housed in the animal facility at the Baylor College of Medicine and were maintained in a 14-h light/10-h dark cyclic environment.

RESULTS

Variants in *TLCD3B* are Associated with Inherited Retinal Degeneration Diseases

To identify novel IRD associated genes, pathogenic variants in known IRD genes were excluded based on targeted exon capture sequencing or virtual gene panel sequencing following whole genome analysis. The remaining unsolved patients were subjected to exome or genome sequencing followed by filtering and annotation, as described in the Materials and Methods section. Probands from three families were identified to harbor rare, likely pathogenic, biallelic variants in *TLCD3B,* a gene encoding a ceramide synthase (Figure 1). This gene was consistently ranked as one of the candidate genes with significantly increased mutation load in our patient cohort with maculopathy by GRIPT (p-value=3.2e-24)[26]. A missense variant (GRCh37 (hg19), NC_000016.9:g.30040796C>T, NM_031478.5:c.166G>A;NP_113666.2:p.(Gly56Ser)) within a transmembrane domain was identified in two of the three families, including the proband A.II.1 and A.II.2. from family A of the State of Minas Gerais, Brazil origin and the proband B.II.1 from family B of the State of Minas Gerais, Brazil origin. The missense variant was likely pathogenic and

associated with disease for the following reasons: first, the genotype of this variant co-segregates with the disease phenotypes within the two families (Figure S1). For family A, the mother of A.II.1 and A.II.2 is asymptomatic and heterozygous for the missense mutation (the father is deceased) while the unaffected siblings are either heterozygous for the variant or wildtype (Figure 1A). Similarly, for family B, the parents and unaffected sibling of B.II.1 are heterozygous carriers (Figure 1A). Genotyping of the SNPs surrounding the variant showed that families A and B share a rare haplotype around the NM_031478.5:c.166G>A;NP_113666.2:p.(Gly56Ser) variant, indicating that it is likely that the variant from these two families is inherited from a founder chromosome region. The three patients in the family A and B (two consanguineous families) share multiple common and rare homozygous SNPs in the region of chr16:29708350–30119379 around NM_031478.5:c.166G>A;NP_113666.2:p.(Gly56Ser) (Table S1). In particular, one of the rare SNP at position 30040796 is exceedingly rare and is only observed twice in the GNOMAD database, making it highly unlikely to happen by chance (with a probability of less than ~1.189E-07). Hence, we reasoned they shared a rare haplotype with a size of about 411,030bp. Second, the affected amino acid is highly conserved in vertebrates from zebrafish to humans (Figure 1B) with a high conservation score (i.e. a VEST3 rankscore of 0.88 and a phastCons100 way vertebrate rankscore of 0.72). Third, this variant was predicted to be damaging by 10 out of 12 *in silico* prediction tools (Table S2). Fourth, this allele was very rare in normal population with population frequency of $7.995X10^{-6}$ in the gnomAD database, with only two heterozygous individuals identified. Additionally, *in silico* modeling of the TLCD3B protein with the c.166G>A variant suggests that the c.166G>A variant substitutes a glycine residue with a serine residue in a transmembrane helix, which would increase the hydrophilicity potentially lead to structural instability of the protein (Figure S2A). The 3D model indicates that Gly56 localizes in a highly hydrophobic cavity (Figure S2B) which could potentially be a substrate binding region which would be disrupted by the c.166G>A variant.

Patient C.IV.3 (GC18125), a 57-year-old male, presented at age 48 with photopsia, photophobia, central vision loss, and a bulls-eye appearance on fundoscopy. He is one of four siblings born to consanguineous union with no family history of ocular disease. He underwent whole genome sequencing, and following exclusion of pathogenic and likely pathogenic variants in an in-house curated virtual gene panel of known and candidate IRD genes, we interrogated rare biallelic loss of function variants (assuming recessive inheritance) in genes that do not harbor homozygous loss of function variants in the ExAC dataset[25]. Two genes, *NUMB* and *TLCD3B,* were found to harbor homozygous frameshift variants. The variant identified in the *NUMB* gene (GRCh37 (hg19) NC_000014.8:g.73746067dup, NM_001005743.1:c.1162dup;NP_001005743.1:p.(Ala388Glyfs*6)) is found in 62/30418 South Asian alleles in the updated gnomAD v2.1 dataset, now including a homozygous individual, and we therefore deemed this variant as unlikely to represent a novel cause of CRD. In addition, a homozygous frameshift variant (GRCh37 (hg19) NC_000016.9:g.30038140del, NM_031478.5:c.234del;NP_113666.2:p.(Gln79Asnfs*43)) in the *TLCD3B* gene was identified. This frameshift variant resides in the third exon of *TLCD3B* (with a total of five exons) and likely leads to non-sense mediated decay. This variant is rare and has not been observed in the gnomAD database. It is

interesting to note that both NM_031478.5:c.166G>A;NP_113666.2:p.(Gly56Ser) and NM_031478.5:c.234del;NP_113666.2:p.(Gln79Asnfs*43) are located within the TLC domain in the N-terminal end (https://www.uniprot.org/uniprot/Q71RH2) (Figure S3C). Taken together, both variants are likely to be loss of function alleles that might impact the TLC domain and function of the protein.

The clinical findings of all affected individuals are summarized in table 1 and phenotypes of all individuals are presented in Figure 2. At the time of publication, all patients present with only the ocular phenotypes presented here and no non-ocular phenotypes have been reported. Family A has two affected siblings, A.II.1 (sister) and A.II.2 (brother), whose parents are second cousins (Figure 1A). A.II.1 and A.II.2 were diagnosed with maculopathy. The proband (Patient A.II.1) is female and presented with progressive loss of central vision and photophobia that significantly impacted their day-to-day life since the age of 30 years. At the age of 30 years, the BCVA was 20/40 for both eyes and decreased to 20/400 at 39 years. Fundus examination disclosed bilateral bull's eye maculopathy without flecks and retinal pigmented epithelium (RPE) atrophy at the periphery (Figure 2A). FAF showed a hypoautofluorescent central lesion with hyperautofluorescent border (Figure 2A). ffERG showed normal scotopic and subnormal photopic responses (Figure 3A). Spectral domain optical coherence tomography (SD-OCT) showed macular photoreceptor loss and disorganization of the inner layers of the retina (Figure 2A).

The younger brother (Patient A.II.2) presented with a severe phenotype, with progressive loss of central vision since the age of 8 (Table 1). Fundus examination disclosed bilateral maculopathy extending to the optic disc with no flecks (Figure 2A). FAF depicted central hypoautofluorescence with hyperautofluorescent border (Figure 2A). The ffERG revealed normal scotopic and reduced photopic responses, consistent with a diagnosis of maculopathy (Figure 3A). SD-OCT showed macular photoreceptor loss and disorganization of the inner layers of the retina (Figure 2A).

Family B has a single affected individual, B.II.1, whose parents are distant cousins (Figure 1A). B.II.1 was diagnosed with CRD. Loss of vision was noted at the age of 24 years. The BCVA was 20/160 in both eyes. Fundus imaging showed loss of foveal reflex and mild macular RPE disturbance (Figure 2B). FAF revealed a hyperautofluorescent macula with sparse hypoautofluorescent small lesions in both eyes and in the left eye, there is a hyperautofluorescent small central lesion (Figure 2B). SD-OCT shows a discontinuous ellipsoid zone (EZ) band with foveal rectification and thinning of the outer nuclear layer (ONL) (Figure 2B). ffERG showed subnormal scotopic and photopic b-waves, consistent with a CRD pattern (Figure 3A).

Family C has a single affected individual diagnosed with CRD, C.IV.3, whose parents are consanguineous (Figure 1A). Patient C.IV.3 has reduced central vision and photophobia (Table 1). Fundus imaging and OCT showed vascular attenuation and loss of the photoreceptor EZ in the macular center (Figure 2C). FAF imaging showed bilateral hyperautofluorescence rings in the macula with hypoautofluorescence in the center (Figure 2C). An ERG at the age of 46 years showed evidence of generalized retinal dysfunction consistent with CRD. Pattern ERG P50 components were undetectable to a standard (15 ×

11 degrees) and large (30 × 22 degrees) checkerboard stimulus field bilaterally, consistent with severe macular involvement. Follow-up ffERGs performed 3.5 years later (Figure 3B) showed no significant change in any of the main ERG components.

TLCD3B is the Most Highly Expressed Ceramide Synthase in the Retina

The restriction of the patient phenotypes to the retina led us to evaluate the expression of *TLCD3B* in various tissue types as well as compare that with the expression profiles of other ceramide synthases. We analyzed the gene expression of ceramide synthase genes *TLCD3A*, *TLCD3B*, and *CERS1–6* in 18 different human tissues (Figure S3A, Table S3) based on RNA-seq data. Consistent with its involvement with cone photoreceptors, *TLCD3B* showed high expression in the adult retina with higher expression in the macular than in the peripheral region (Figure S3A, Table S3). Differential expression of *CERSs* across different tissues is observed with *CERS4* showing the highest expression in the adult retina (Figure S3A, Table S3). *CERS5* and *CERS6* show higher expression in fetal retina (Figure S3A, Table S3). *CERS2* is highly and prevalently expressed in other tissues (Figure S3A, Table S3). Although there are three isoforms annotated for *TLCD3B* by NCBI ReSeq gene annotation, the RNA-seq of normal human retina showed that NM_031478.5 is the major isoform in the retina (Figure S3B). Both variants identified in this study affect conserved exons (Figure S3B) and exist within the TLC domain essential for ceramide synthesis (Figure S3C). Consistent with the expression results observed in human, staining for Tlcd3b reveals ubiquitous expression throughout all layers of the neural retina in mice (Figure S4C). These results suggest that *TLCD3B* might play an important role in adult retina.

Tlcd3b Knockout Mice Recapitulate the Patient Phenotype

A *Tlcd3b* knockout mouse generated by KOMP2 (Figure S4A) was obtained for use to further confirm *TLCD3B* as a retinal degeneration gene and establish a model to further study its role in the retina. The knockout of *Tlcd3b* was evaluated at DNA (Figure S4B) and protein level (Figure S4C). Staining for the Tlcd3b protein shows loss of expression in the *Tlcd3b*$^{KO/KO}$ mouse retina (Figure S4C). Despite the high expression of *TLCD3B* in testes (Figure S3A) the *Tlcd3b*$^{KO/KO}$ male mice were fertile. Following confirmation of the knockout allele, characterization studies of the retina were conducted to evaluate a retinal degeneration phenotype. ERG analysis showed reduced scotopic and photopic b-wave amplitude in 7-month-old *Tlcd3b*$^{KO/KO}$ mice (n=5) compared to control mice (n=7) (Figure 4A). Scotopic a-wave ERGs showed a normal response of rod photoreceptors in the *Tlcd3b*$^{KO/KO}$ mice (Figure 4A left), indicating largely normal rod photoreceptor activity. There was a 25% reduction in scotopic b-wave amplitude for *Tlcd3b*$^{KO/KO}$ mice at maximum stimulus intensity (Figure 4A). The reduced scotopic b-wave is indicative of dysfunction occurring post-phototransduction or at the level of bipolar cells in the *Tlcd3b*$^{KO/KO}$ mice [27]. Photopic ERGs showed a 40% reduction in b-wave amplitude at maximum stimulus intensity in *Tlcd3b*$^{KO/KO}$ mice compared to control mice (Figure 4A right), indicating dysfunctional cones. These results indicate that *Tlcd3b*$^{KO/KO}$ mice exhibit significant cone dysfunction at 7 months-of-age.

Since the ERGs indicated potential defects in the photoreceptors and interneurons, hematoxylin and eosin (H&E) staining was conducted on retinal cross-sections to evaluate

the retinal morphology (Figure 4B). H&E staining of retinal sections showed that there is about a 20% reduction in the ONL thickness (Figure 4C) and number of nuclei (Figure S5A) and insignificant thinning of the inner nuclear layer (INL) (Figure 4D) across the retina of the *Tlcd3b*$^{KO/KO}$ mice (n=3) compared to controls (n=6) at 7 months-of-age. Rod-bipolar cells were evaluated by Pkcα staining (Figure S5B), and no significant changes were observed to cell number or morphology. The level of reduction of the ONL thickness suggests that rod photoreceptors are degenerating as well, though not yet detectable by ERG. To examine if the cones are degenerated, Peanut agglutinin (PNA), which specifically binds cone photoreceptors, was used to stain the retina [28]. Retinal cross-sections taken from 7-month-old mice show reduced number of cones by PNA staining in the inner and outer segment in the mutant retina compared to wildtype retina (Figure 4E). The cone density differs across the retina[29], therefore, the cone degeneration phenotype cannot be accurately determined from retinal cross-sections alone. To evaluate if the cone density differs across the retina in *Tlcd3b*$^{KO/KO}$ mice compared to controls, PNA staining was conducted on retinal whole mounts (Figure 4F). PNA-positive cones were counted in the dorsonasal, dorsotemporal, ventronasal, and ventrotemporal regions of PNA-stained retinal whole mounts of 7-month-old *Tlcd3b*$^{KO/KO}$ mice (n=3) and control mice (n=3) (Figure 4F). Overall, there was a 30% loss of cones in mutant retina compared to wildtype retina with significant loss in the dorsotemporal, ventronasal, and ventrotemporal areas (Figure 4G).

DISCUSSION

We report rare biallelic variants in *TLCD3B* in four affected individuals from three unrelated families with retinal dystrophy. Variants in *TLCD3B* have not been previously implicated in any human disease, the data presented here demonstrate that damaging variants in *TLCD3B* are associated with recessive CRD and maculopathy. In the present study, we show that the affected individuals diagnosed with either CRD or maculopathy had homozygous recessive pathogenic variants in *TLCD3B.* They showed clinical signs of cone photoreceptor degeneration by fundus imaging and showed ERG evidence of predominant cone system dysfunction. Fundus imaging revealed significant degeneration of the macula, which is enriched in cone photoreceptors, while ffERGs confirmed generalized (peripheral) cone system involvement. In addition, we have shown in mice by ERGs and quantification of cone photoreceptors that the phenotype due to homozygous knockout of *Tlcd3b* is consistent with photoreceptor degeneration. Since mice lack a macular region in the retina, the cone degeneration and ERG phenotype approximates to the human phenotype. Although ERGs did not reveal generalized rod photoreceptor dysfunction in the *Tlcd3b* knockout mouse, the level of reduction in the ONL thickness suggests that rod photoreceptors are also degenerating. The eye-specific phenotype observed is consistent between patients and the mouse model. These results show that *Tlcd3b* knockout mice effectively recapitulate the progressive phenotype observed in human patients and confirms the association of rare damaging variants in *TLCD3B* with inherited retinal degeneration, and shows that TLCD3B is required for retinal function and survival. While pathogenic variants in *TLCD3B* account for only a small proportion of retinal degeneration patients, this study and the *Tlcd3b* knockout mouse described here will provide a foundation for future ceramide and ceramide synthase studies.

It is interesting to note that both inter and intra family variation in the severity of clinic phenotype is observed in patients from families A and B who share the same *TLCD3B* allele, c.166G>A. The phenotypes of the three patients, A.II.1, A.II.2, and B.II.1, have similar clinical presentations with significant macular involvement, indicative of cone-rod degeneration. The reason for the difference in severity between family A and B and the differences between the patients within family A is not clear. However, such clinical inter- and intra-family variation is frequently observed in CRD patients. The mechanism underlying the clinical variation is not clear. One potential explanation for the variability could be differences in the genetic background where other variants in the patient genome might contribute to the variation in the clinical presentation. As shown in Table S4, potential deleterious variants in known IRD genes identified from WES/WGS data for each patient are examined. However, comparison of the variant lists for A.II.1 and A.II.2 does not yield obvious candidate variants that could explain the variation. Patient C.IV.3 exhibits a similar phenotype to the other three patients but has a different causative allele, c.234DelG, which causes a frameshift and early stop codon. While patient C.IV.3 does not have the most severe changes to the retina based on fundus imaging, they have more severe defects in their vision (based on BCVA) compared to the patients in family A.

The reduced murine scotopic ERG b-wave coupled with a normal scotopic a-wave is an intriguing phenotype. It is indicative of post-phototransduction dysfunction which could be due to either rod photoreceptor or interneuron dysfunction, likely contributed to by bipolar cells. To better understand this potential phenotype, a comprehensive histological analysis of the interneurons is needed to evaluate the organization and possible degeneration of these cells. Preliminary staining to evaluate the interneuron cells indicated that rod bipolar cells were not significantly affected in organization or number, but other cell types may be affected, such as cone bipolar cells, and need further evaluation. Evaluating retinal function and morphology at later time points will help to characterize the role rod photoreceptors in the pathology of this mouse model and determine if the rod photoreceptors alone can explain the scotopic ERG b-wave phenotype or if both rods and bipolar cells contribute.

Although the importance of ceramide homeostasis in retinal neurons has been implicated, the lack of a genetics model makes it challenging to probe the underlying mechanism. TLCD3B synthesizes C16-, C18-, and C20-ceramides[22] and we demonstrate it to be the most highly expressed ceramide synthase in the retina relative to other ceramide synthases. Previous ceramide synthase knockout mouse models have not exhibited retinal degeneration phenotypes[18], nor have other ceramide synthases been linked to retinal degeneration. While there is redundancy in the ceramide synthase products, with several CERSs generating some of the same products as TLCD3B, there may still be an overall reduction in the ceramide level or reduction in the level of specific ceramides in the retina resulting in degeneration. We will leverage the Tlcd3b knockout mouse to evaluate the ceramide profile changes in the retina to gain insight to the mechanism of disease. We speculate that the loss of TLCD3B will result in both a reduction in total ceramide as well as a shift in the relative ceramide ratios. Future studies will examine the role of TLCD3B in ceramide synthesis *in vivo* and its involvement in maintenance of photoreceptor function and survival. The *Tlcd3b*$^{KO/KO}$ model will also be used to evaluate the efficacy of several therapeutic interventions, including gene replacement therapy and exogenous ceramide supplementation.

Supplementary Material

Refer to Web version on PubMed Central for supplementary material.

ACKNOWLEDGMENTS

First, we wish to thank the patients and families who kindly participated in this study. This work was supported by grants from Fight for Sight (UK) (Early Career Investigator Award to G.A.), Moorfields Eye Charity, NIHR Bioresource – Rare Disease Consortium, the NIHR BRC at Great Ormond Street Hospital for Child Health, and the National Institute for Health Research Biomedical Research Centre at Moorfields Eye Hospital, UCL Institute of Ophthalmology and Cambridge University Hospitals, the Competitive Renewal Grant of Knights Templar Eye Foundation to J.W., and grants from the National Eye Institute (EY022356, EY018571, EY002520), Retinal Research Foundation, and NIH shared instrument grant S10OD023469 to R.C.

REFERENCES

1. Ellingford JM, Barton S, Bhaskar S, et al. Molecular findings form 537 individuals with inherited retinal disease. Journal of Medical Genetics 2016;53(11):761–67. doi: 10.1136/jmedgenet-2016-103837 [PubMed: 27208204]
2. Gill JS, Georgiou M, Kalitzeos A, et al. Progressive cone and cone-rod dystrophies: Clinical features, molecular genetics and prospects for therapy. British Journal of Ophthalmology 2019(5):711–20. doi: 10.1136/bjophthalmol-2018-313278
3. Eagle RC. Mechanisms of Maculopathy. Ophthalmology 1984;91(6):613–25. [PubMed: 6205340]
4. Hannun Y, Obeid L. Principles of bioactive lipid signalling: Lessons from sphingolipids. Nature Reviews Molecular Cell Biology 2008;9(2):139–50. doi: 10.1038/nrm2329 [PubMed: 18216770]
5. Kitatani K, Idkowiak-Baldys J, Hannun YA. The sphingolipid salvage pathway in ceramide metabolism and signaling. Cell Signaling 2008;20(6):1010–18.
6. Ferlazzo E, Italiano D, An I, et al. Description of a Family with Novel Progressive Myoclonus Epilepsy and Cognitive Impairment. Movement Disorders 2009;24(7):1016–22. doi: 10.1002/mds.22489 [PubMed: 19243074]
7. Laviad EL, Albee L, Pankova-Kholmyansky I, et al. Characterization of Ceramide Synthase 2 Tissue Distribution, Substrate Specificity, and Inhibition by Sphingosine 1-Phosphate. The Journal of Biological Chemistry 2008;283:5677–84. [PubMed: 18165233]
8. Mizutani Y, Kihara A, Igarashi Y. Mammalian Lass6 and its related family members regulate synthesis of specific ceramides. Biochemical Journal 2005;390(1):263–71.
9. Riebeling C, Allegood JC, Wang E, et al. Two Mammalian Longevity Assurance Gene (LAG1) Family Members, trh1 and trh4, Regulate Dihydroceramide Synthesis Using Different Fatty Acyl-CoA Donors. The Journal of Biological Chemistry 2003;278:43452–59. [PubMed: 12912983]
10. Zhao L, Spassieva S, Jucius T, et al. A Deficiency of Ceramide Biosynthesis Causes Cerebellar Purkinje Cell Neurodegeneration and Lipofuscin Accumulation. PLoS Genetics 2011;7(5) doi: 10.1371/journal.pgen.1002063
11. German O, Miranda G, Abrahan C, et al. Ceramide is a mediator of apoptosis in retina photoreceptors. Investigative ophthalmology and visual science 2006;47(4):1658–68. doi: 10.1167/iovs.05-1310 [PubMed: 16565407]
12. Prado Spalm F, Vera M, Dibo M, et al. Ceramide induces the death of retina photoreceptors through activation of parthanatos. Molecular Neurobiology 2018 doi: 10.1007/s12035-018-1402-4
13. Sanvicens N, Cotter T. Ceramide is the key mediator of oxidative stress-induced apoptosis in retinal photoreceptor cells. Journal of Neurochemistry 2006;98(5):1432–44. doi: 10.1111/j.1471-4159.2006.03977.x [PubMed: 16923157]
14. Ranty M, Carpentier S, Cournot M, et al. Ceramide production associated with retinal apoptosis after retinal detachment. Graefe's Archive for Clinical and Experimental Ophthalmology 2009;247(2):215–24. doi: 10.1007/s00417-008-0957-6
15. Strettoi E, Gargini C, Novelli E, et al. Inhibition of ceramide biosynthesis preserves photoreceptor structure and function in a mouse model of retinitis pigmentosa. Proceedings of the National Academy of Science 2010;107(43):18706–11. doi: 10.1073/pnas.1007644107

16. Eckl K, Tidhar R, Thiele H, et al. Impaired Epidermal Ceramide Synthesis Causes Autosomal Recessive Congenital Ichthyosis and Reveals the Importance of Ceramide Acyl Chain Length. Journal of Investigative Dermatology 2013;133(9):2202–11. doi: 10.1038/jid.2013.153

17. Vanni N, Fruscione F, Ferlazzo E, et al. Impairment of Ceramide Synthesis Causes a Novel Progressive Myoclonus Epilepsy. Annals of Neurology 2014;76(2):206–12. doi: 10.1002/ana.24170 [PubMed: 24782409]

18. Brüggen B, Kremser C, Bickert A, et al. Defective ceramide synthases in mice cause reduced amplitudes in electroretinograms and altered sphingolipied composition in retina and cornea. European Journal of Neuroscience 2016;44(1):1700–13. doi: 10.1111/ejn.13260

19. Avela K, Sankila EM, Seitsonen S, et al. A founder mutation in CERKL is a major cause of retinal dystrophy in Finland. Acta Ophthalmol 2018;96(2):183–91. doi: 10.1111/aos.13551 [published Online First: 2017/10/27] [PubMed: 29068140]

20. Fathinajafabadi A, Perez-Jimenez E, Riera M, et al. CERKL, a retinal disease gene, encodes an mRNA-binding protein that localizes in compact and untranslated mRNPs associated with microtubules. PLoS One 2014;9(2):e87898. doi: 10.1371/journal.pone.0087898 [published Online First: 2014/02/06] [PubMed: 24498393]

21. Hu X, Lu Z, Yu S, et al. CERKL regulates autophagy via the NAD-dependent deacetylase SIRT1. Autophagy 2019;15(3):453–65. doi: 10.1080/15548627.2018.1520548 [published Online First: 2018/09/13] [PubMed: 30205735]

22. Yamashita-Sugahara Y, Tokuzawa Y, Nakachi Y, et al. Fam57b (Family with Sequence Similarity 57, Member B), a Novel Peroxisome Proliferator-activated Receptor γ Target Gene That Regulates Adipogenesis through Ceramide Synthesis. Journal of Biological Chemistry 2012;288(7):4522–37. doi: 10.1074/jbc.m112.440792

23. Li H, Durbin R. Fast and accurate short read alignment with Burrows-Wheeler transform. Bioinformatics 2009;25(14):1754–60. doi: 10.1093/bioinformatics/btp324 [published Online First: 2009/05/20] [PubMed: 19451168]

24. Wang F, Wang H, Tuan HF, et al. Next generation sequencing-based molecular diagnosis of retinitis pigmentosa: identification of a novel genotype-phenotype correlation and clinical refinements. Hum Genet 2014;133(3):331–45. doi: 10.1007/s00439-013-1381-5 [published Online First: 2013/10/25] [PubMed: 24154662]

25. Carss KJ, Arno G, Erwood M, et al. Comprehensive Rare Variant Analysis via Whole-Genome Sequencing to Determine the Molecular Pathology of Inherited Retinal Disease. The American Journal of Human Genetics 2017;100:75–90. [PubMed: 28041643]

26. Wang J, Zhao L, Wang X, et al. GRIPT: a novel case-control analysis method for Mendelian disease gene discovery. Genome Biol 2018;19(1):203. doi: 10.1186/s13059-018-1579-x [published Online First: 2018/11/28] [PubMed: 30477545]

27. Baba K, Piano I, Lyuboslavsky P, et al. Removal of clock gene Bmal1 from the retina affects retinal development and accelerates cone photoreceptor degeneration during aging. PNAS 2018;115(51):13099–104. [PubMed: 30498030]

28. Blanks JC, Johnson LV. Specific Binding of Peanut Lectin to a Class of Retinal Photoreceptor Cells A Species Comparison. Investigative ophthalmology and visual science 1984;25(5)

29. Ortín-Martínez A, Nadal-Nicolás FM, Jiménez-López M, et al. Number and distribution of mouse retinal cone photoreceptors: Differences between an albino (Swiss) and a pigmented (C57/BL6) strain. PLoS ONE 2014;9(7):1–12.

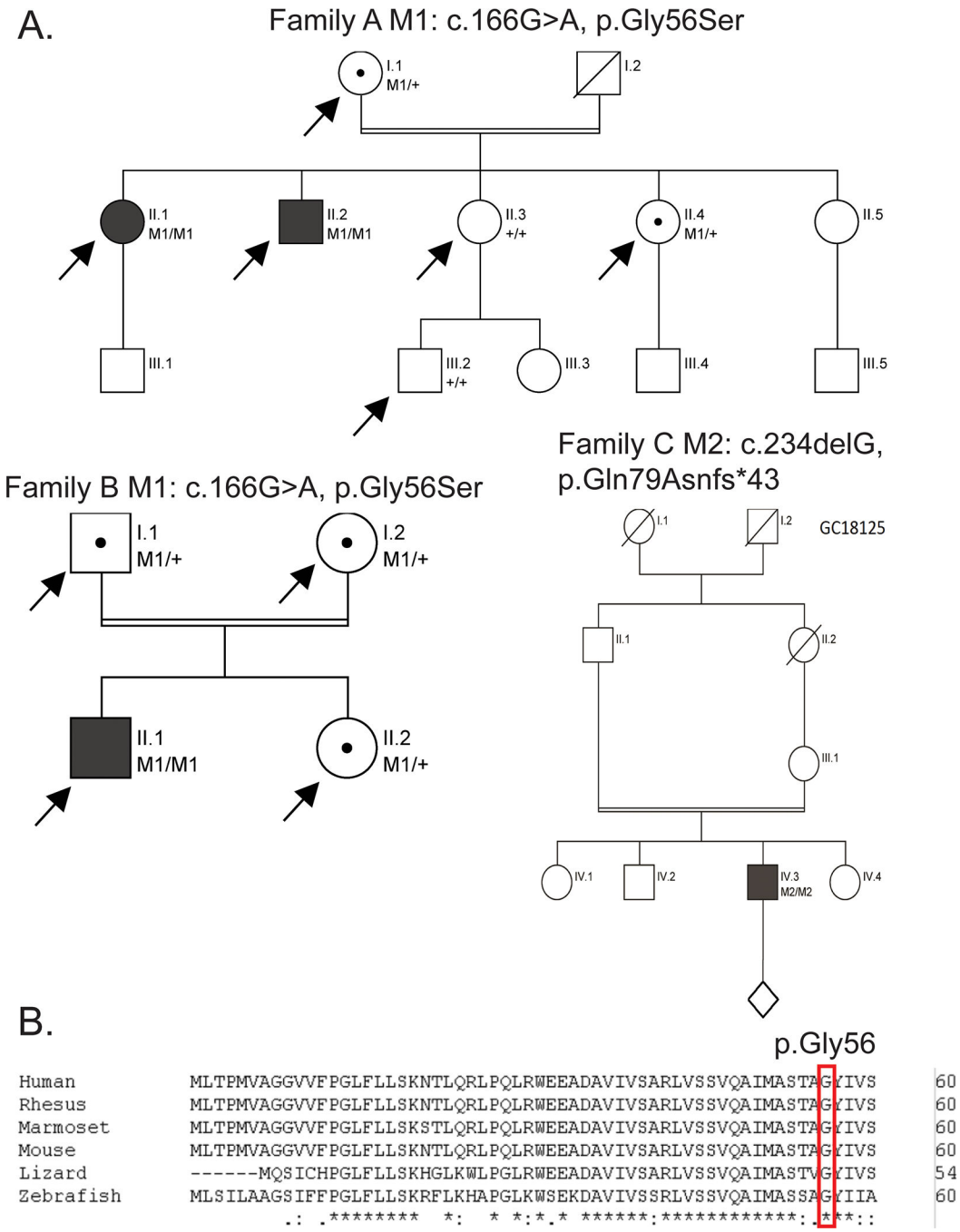

Figure 1.

Autosomal recessive cone-rod dystrophy (CRD) or maculopathy families and associated *TLCD3B* variants. (A) Pedigrees of all families with CRD or maculopathy in this study (family A to C). Proband II.1 and II.2 from the family A both with maculopathy are homozygous for a missense variant (M1/M1). Proband II.1 from the family B with cone-rod dystrophy is also homozygous for this missense variant (M1/M1). Proband IV.3 from the family C with CRD is homozygous for a frameshift variant (M2/M2). The index individuals were validated by sanger sequencing. (B) Protein sequence alignment showed p.G56 (M1) is

highly conserved across species. Arrows indicate exome or genome sequencing was performed for that individual, filled in individuals indicates retinal dystrophy phenotype, dots indicate individual is a confirmed carrier of the allele, diagonal lines indicate individual is deceased.

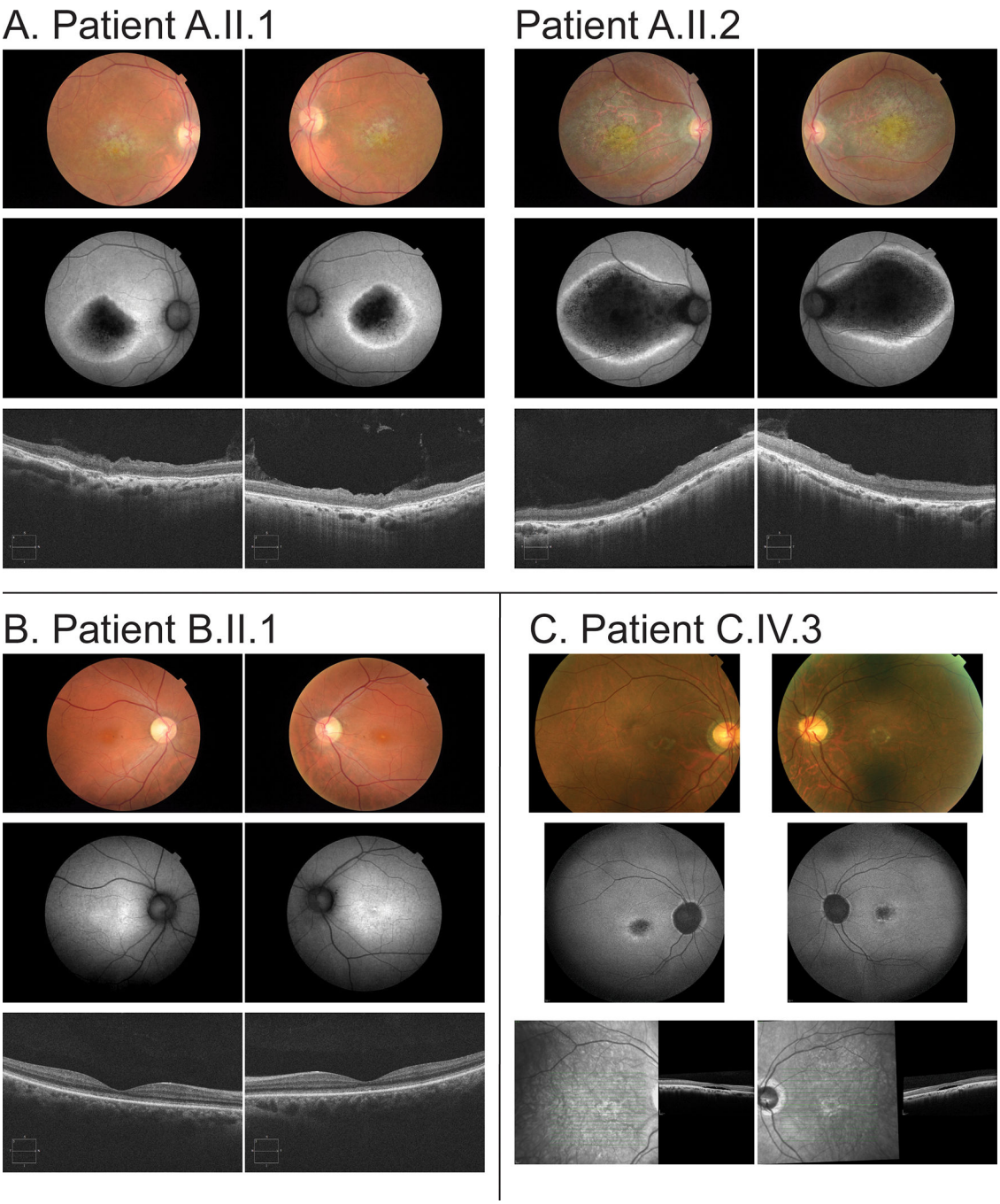

Figure 2.

The clinical phenotype for each patient indicates degeneration of the central (macular) and outer retinal layers. *Top* Color fundus imaging, *middle* short-wavelength autofluorescence fundus imaging, *bottom* optical coherence tomography (OCT) for each of (A, left) Patient A.II.1 (A, right) Patient A.II.2 (B) Patient B.I.1 and (C) Patient C.IV.3. In A, both patients exhibit marked loss of autofluorescence due to atrophy of both photoreceptors and retinal pigmented epithelium (RPE). In B the degeneration is less severe with loss of foveal volume and disruption of the ellipsoid line at the fovea, with consequent increase in the underlying

autofluorescence from the intact RPE. In C there is loss of the outer foveal structure replaced with a small volume of subretinal fluid. In all patients the degeneration is compatible with predominant cone photoreceptor involvement.

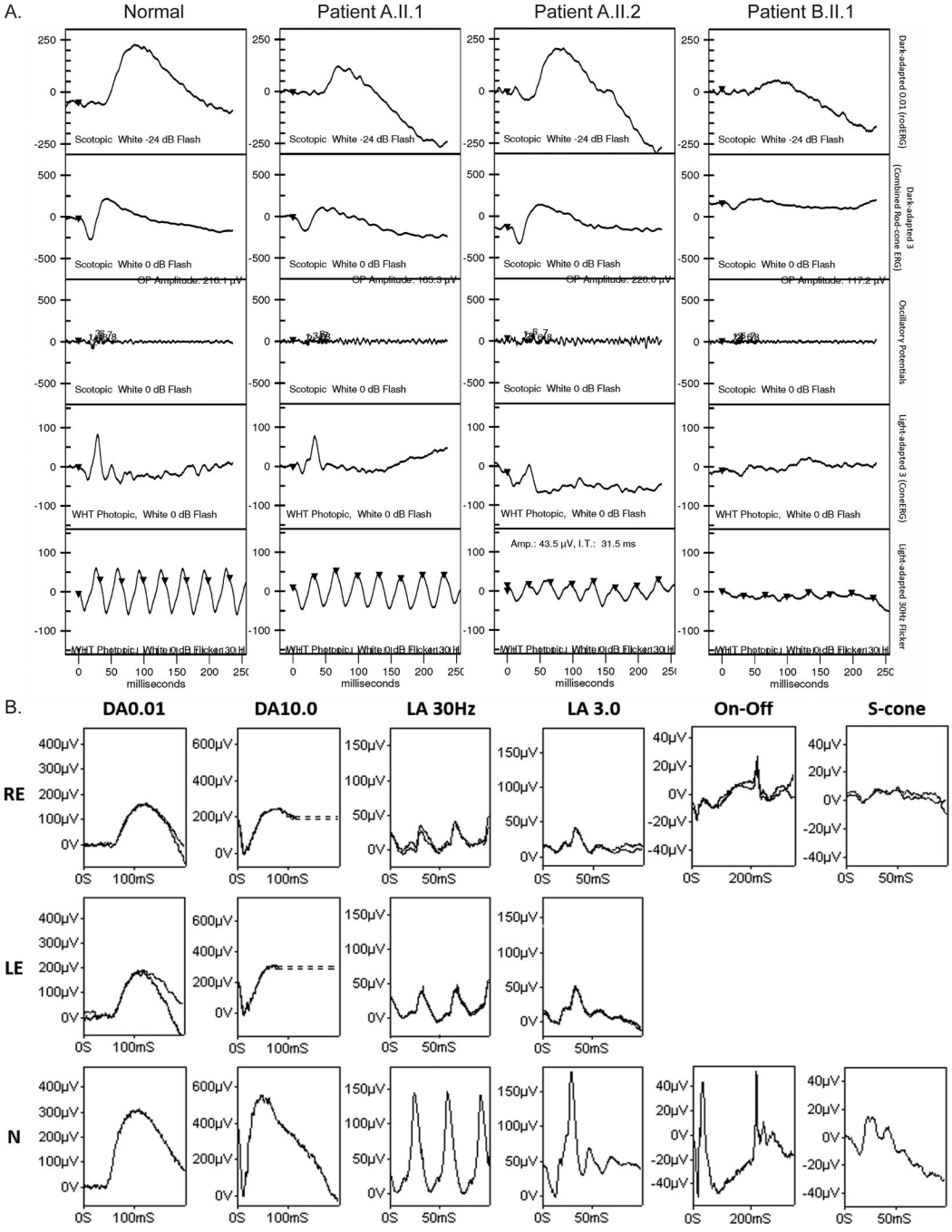

Figure 3.

The full-field electroretinographies (ffERGs) indicate generalized cone system dysfunction with rod photoreceptor involvement in some patients. (A) ERGs were conducted in Brazil and show representative ffERGs in a normal subject and patients A.II.1, A.II.2, and B.II.1. Recordings showed a high degree of inter-ocular symmetry, so only one eye is shown. The ERG findings indicate macular dystrophy in patients A.II.1 and A.II.2, with subnormal photopic responses in patient A.II.2; and cone-rod dystrophy in patient B.II.1. (B) ERG was conducted in the UK. Data recorded from the right (RE) and left (LE) eye of patient C.IV.3

are compared with recordings from a representative unaffected control subject (N). Broken lines replace blink/eye movement artefacts occurring after ERG b-waves for clarity. The ERG findings indicate generalized cone system dysfunction with mild rod photoreceptor involvement bilaterally, in keeping with cone-rod dystrophy. Abnormalities of photopic On- and Off ERG components and S-cone ERGs are consistent with cone dysfunction affecting postreceptoral signaling to cone On and Off bipolar cells. All recordings were reproducible.

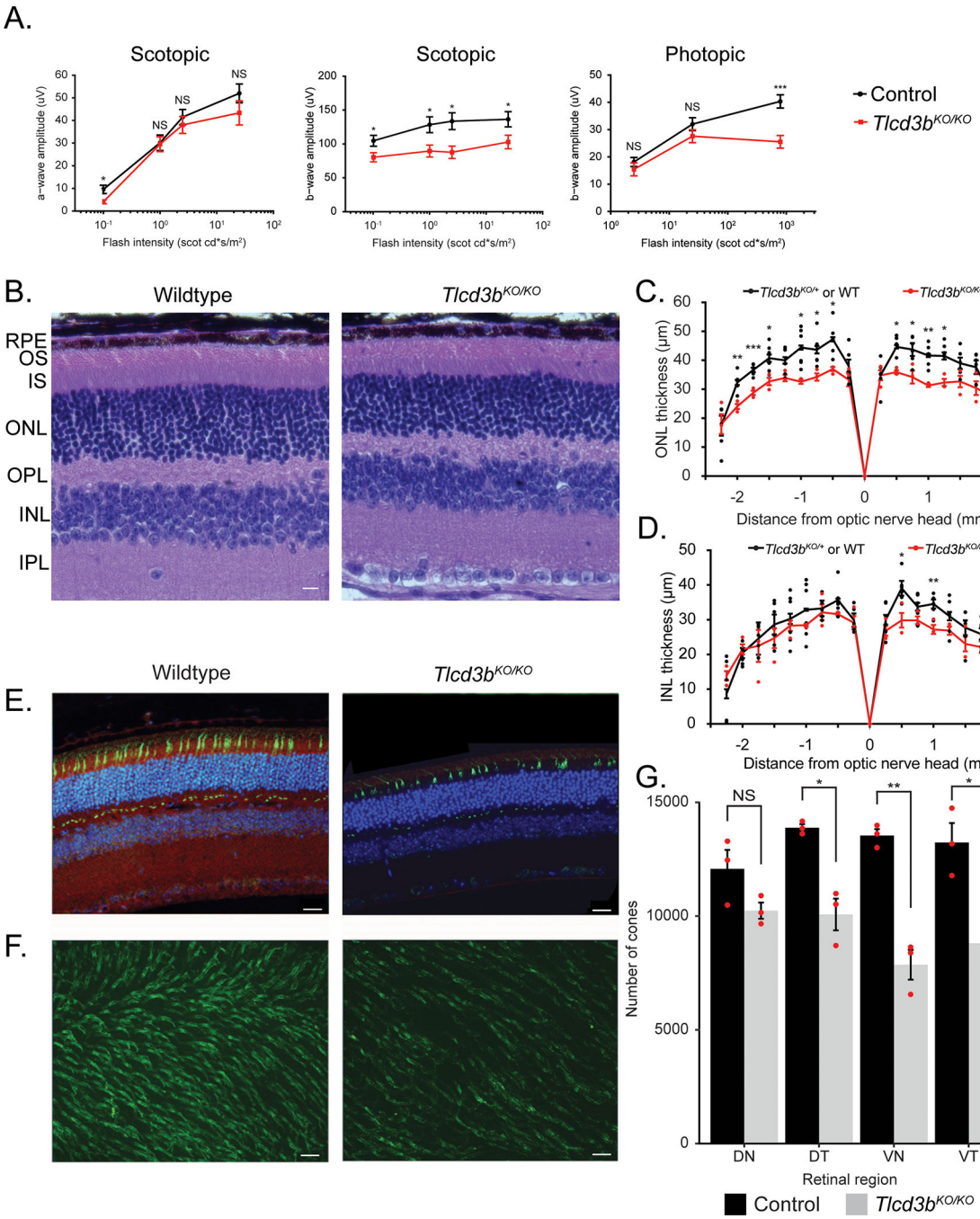

Figure 4.

Tlcd3b knockout mice exhibit retinal degeneration and significant loss of cone photoreceptors. (A) Electroretinography analysis shows scotopic a-wave is unaffected (p = 0.3) but the scotopic b-wave (p = 0.01) and photopic b-wave (p = 0.008) amplitudes are reduced in 7-month-old *Tlcd3b*$^{KO/KO}$ mice (n=5) compared to *Tlcd3b*$^{+/KO}$ or wild-type control mice (n=7). (B) Hematoxylin and eosin staining of retinal cross-sections shows overall retinal thinning in *Tlcd3b*$^{KO/KO}$ mice compared to wildtype control mice at 7 months-of-age. Scale bar = 20 µm. RPE=retinal pigment epithelium, ONL=outer nuclear

layer, INL=inner nuclear layer, OPL=outer plexiform layer, IPL=inner plexiform layer, GCL=ganglion cell layer, OS=outer segment, IS=inner segment. (C) ONL measurements show a 20% reduction ($p = 0.003$) in ONL thickness in *Tlcd3b*$^{KO/KO}$ mice ($n = 3$) compared to wildtype or *Tlcd3d*$^{+/KO}$ control mice ($n = 6$) at 7 months of age ($p = 0.002$). Each dot represents an individual data point plotted over mean ± SEM. (D) INL measurements show no significant changes ($p = 0.1$) in INL thickness in *Tlcd3b*$^{KO/KO}$ mice ($n=3$) compared to wildtype or *Tlcd3b*$^{+/KO}$ control mice ($n=6$) at 7 months of age. Each dot represents an individual data point plotted over mean ± SEM. (E) Co-staining of Fam57b preabsorbed antibody (red) and peanut agglutinin (PNA) (green) shows expression of *Tlcd3b* in cone photoreceptors. (E, F) PNA staining (green) shows loss of cones in *Tlcd3b*$^{KO/KO}$ retina compared to wildtype in retinal sections (E) and retinal wholemounts (F). Scale bar = (E) 20 μm, (F) 50 μm. (G) Cones were counted in the dorsonasal (DN), dorsotemporal (DT), ventronasal (VN), and ventrotemporal (VT) regions of (F) PNA-stained (green) retinal wholemounts of 7-month-old *Tlcd3b*$^{KO/KO}$ mice ($n = 3$) and control mice ($n = 3$). (F, G) The number of cones is significantly reduced in the *Tlcd3b*$^{KO/KO}$ retina compared to controls ($p = 0.003$). Data is expressed as average number of cones per mm^2 (mean ± SEM). Individual data points were plotted in addition to statistics. NS = not significant, *$p<0.05$, **$p<0.01$, ***$p<0.001$.

Table 1.

Clinical phenotypes of affected individuals with homozygous *TLCD3B* mutations.

Affected Individual	Age at Diagnosis	Diagnosis	*TLCD3B* Variant	Visual Acuity (Right)	Visual Acuity (Left)	Central Vision Loss	Additional Notes
A.II.1	16	Maculopathy	c.166G>A p.Gly56Ser	5/200	5/100	+	Photophobia
A.II.2	8	Maculopathy	c.166G>A p.Gly56Ser	5/100	5/100	+	Photophobia
B.II.1	24	CRD	c.166G>A p.Gly56Ser	5/60	5/60	+	Photophobia
C.IV.3	45	CRD	c.234delG p.Gln79Asnfs*43	2/60	2/60	+	Ishihara Nil, Photophobia